Soft Matter

Accepted Manuscript

ROYAL SOCIETY OF CHEMISTRY

www.rsc.org/softmatter

Aggregation dynamics of molecular bonds between compliant materials

Hongyuan Jiang[1], Jin Qian[2,*], Yuan Lin[3], Yong Ni[1] and Linghui He[1]

[1] Department of Modern Mechanics, CAS Key Laboratory of Mechanical Behavior and Design of Materials, University of Science and Technology of China, Hefei, Anhui 230026, China

[2] Department of Engineering Mechanics, Soft Matter Research Center, Zhejiang University, Hangzhou, Zhejiang 310027, China

[3] Department of Mechanical Engineering, The University of Hong Kong, Hong Kong SAR, China

* To whom correspondence should be addressed. E-mail: jqian@zju.edu.cn.

Abstract

In this paper, we develop a mechanochemical modeling framework in which the spatial-temporal evolution of receptor-ligand bonds takes place at the interface between two compliant media in the presence of an externally applied tensile load. Bond translocation, dissociation and association occur simultaneously, resulting in dynamic aggregation of molecular bonds that is regulated by mechanical factors such as material compliance and applied stress. The results show that bond aggregation is energetically favorable in the out-of-equilibrium process with convoluted time scales from bond diffusion and reaction. Material stiffness is predicted to contribute to adhesion growth and an optimal level of applied stress leads to the maximized size of bond clusters for integrin-based adhesion, consistent with related experimental observations on focal adhesions of cell-matrix interaction. The stress distribution within bond clusters is generally non-uniform and governed by the stress concentration index.

Keywords

cell-matrix adhesion; receptor-ligand bond; integrin; clustering; diffusion; kinetic reaction

1 Introduction

The adhesive interaction between cells and extracellular matrices (ECMs) plays a pivotal role in regulating cellular processes such as cell spreading, migration, differentiation and morphogenesis. In transmitting mechanical forces at the interface, cell-matrix adhesion has been found to operate by assembling into discrete focal contacts, largely mediated by clusters of molecular bonds formed between transmembrane integrins on cells and their ligands on ECM surfaces.[1] The focal adhesion (FA) spots usually exhibit sizes from several hundred nanometers to a few micrometers, which may consist of hundreds to thousands of integrin-ligand bonds.[2,3] The formation of densely clustered molecular bonds around micrometer-size has been observed in not only cell-matrix adhesions but cell-cell junctions.[4]

Why are focal adhesions discrete by nature with their sizes falling into a narrow range around the micrometer scale? The mounting experimental evidences on discontinuous distribution and characteristic size of focal adhesions have attracted attention of researchers in the past decade and led to significant efforts from theoretical point of view. Based on the solution to a one-step master equation, Erdmann and Schwarz demonstrated that molecular clusters below a critical size behave like a single bond with a limited lifetime while those above the critical size survive over a much prolonged time owing to the collective or cooperative effect of clustering.[5,6] Therefore, bond clustering leads to augment in adhesion size and contributes to the stability of bond ensemble: bond clusters smaller than a lower-bound are subjected to frequent turnover, while sufficiently large clusters tend to have a much longer lifetime similar to stable focal adhesions. Qian et al.,[7,8] as well as Lin and Freund,[9] extended the analysis to including the effects of material compliance and non-uniform stress distribution on the stability of a single or an array of adhesion clusters under tensile load, with results predicting a window of intermediate cluster size for relatively stable adhesion and an optimal cluster size for maximum strength.

In this sense, the size of focal adhesion is lower-bounded due to stability issue and upper-bounded as long as material compliance is considered.

Indeed, the mechanical properties of extracellular matrices are increasingly recognized as important parameters in determining the size, density and distribution of integrin-ligand bond clusters as well as their adhesion performance, as evidenced by cellular responses to different types of polyacrylamide- and alginate-based gels during the past two decades.[10-12] Large patches of focal adhesions are usually formed on sufficiently rigid substrates, while too compliant matrices result in small point-like adhesion structures.[13,14] Moreover, cells tend to migrate toward stiffer region when cultured on an elastically heterogeneous substrate.[15,16] The profound effects of material rigidity on cell-matrix adhesion may also be raised from the intracellular side, which received less attention in literature, since the elastic modulus of cytoskeleton can change over several orders of magnitude in response to different levels of myosin-II-driven contractility.[17,18]

The focal adhesions between cells and the opposing ECM surfaces, consisting of multiple receptor-ligand bonds, are generally exposed to tractions forces induced by different physical interactions such as those due to blood flow or other external environments, as well as those generated by cell's own contractile machinery. Experiments have also revealed that the size of mature FAs can reversibly increase or decrease in proportion to the magnitude of applied tensile force, with force per unit area (i.e., stress) maintained near a constant value around kilopascal level irrespective of cell type.[19,20] The role of this characteristic level of traction acting at the cell-ECM interface is intriguing in the formation of focal adhesions.

The aforementioned experimental observations seem to suggest a coherent interplay of adhesion size, material stiffness and mechanical stress in FA formation and function at the cell-ECM interface,

while the issues of how characteristic size and adhesion strength of FAs are influenced by substrate rigidity and applied load were often treated separately in existing studies. For example, the effects of cluster size on adhesion stability have been investigated in the presence of substrate deformation, with results showing that optimal adhesion lifetime is achieved only at intermediate adhesion sizes,[7,8] without addressing how these micrometer-sized clusters are formed at the interface over time. On the other side, theoretical and numerical approaches have been developed to study the temporal evolution of species separation owing to the mismatch between short and long adhesion molecules,[21-23] with implications in patterned domain formation in T-cell receptor-based or integrin-based adhesion; Wang and Gao have performed a stability analysis and theoretically showed that the uniform distribution of interfacial molecular bonds is energetically unfavorable for the coexistence of receptor-ligand bonds and glycocalyx molecules at the compliant interface, predicting that bond clusters with a dominating length scale grow the fastest.[24] However, these studies on dynamic aggregation process of molecular bonds ought to be accompanied by the modeling efforts of adhesion strength and/or kinetic descriptions of bond dissociation and association. Thus, the current theoretical understanding on the subject is still fragmented.

It should be noted that focal adhesion between cell and matrix is a complex structure, where more than 200 different proteins including talin, paxilin, vinculin, zyxin as well as integrin are at work.[25] Increasing biological complexities may be crucial for proper modeling of FA formation and mechanosensitivity.[26] Before the mystery is fully clarified by experiments, one way to proceed is to make some reasonable assumptions and look for possible consistencies or contradictions in subsequent research. The present work aims to develop a quantitative coupling framework for understanding how mechanical and chemical cues modulate the motion and reaction of molecular bonds at the compliant interface between opposing materials. Essentially, bond clustering is considered as an energy-driven

process in a competition between various time scales rooted in lateral diffusion and kinetic reaction of the involved molecular bonds. This study extends the previous modeling framework by Wang and Gao[24] in several aspects: i) the previous assumption of plane-strain configuration is released and in this study bond aggregation occurs at the interface between three dimensional materials; ii) the present model provides not only the ultimate state of adhesion that is energetically favorable, but the real-time evolution of the entire aggregation process of how these bond clusters are formed; iii) the binding and unbinding kinetics of molecular bonds are also included in the current analysis.

2 Theory

Here we focus on an idealized model aiming to interconnect the major aspects that are important in the aggregation dynamics of molecular bonds, with special attention to the effects of material stiffness, applied stress as well as bond kinetics on the emerging size of temporal adhesion patterning. Consider two semi-infinite elastic bodies joined by receptor-ligand bonds at the interface against a remotely applied stress σ_0 (Fig. 1a). E_1, ν_1 and E_2, ν_2 are Young's modulus and Poisson's ratio of the two materials, respectively. Following the convention of contact mechanics, the elastic deformation from both materials can be combined together by defining a reduced elastic modulus E^* through the relation:[27]

$$1/E^* = \left(1-\nu_1^2\right)/E_1 + \left(1-\nu_2^2\right)/E_2 . \tag{1}$$

It is assumed that individual receptor-ligand bonds can transit between a linked state and a ruptured state, which will be described as rate processes in the following sections (Fig. 1b), and they can laterally translocate across the two-dimensional interface (Fig. 1c). Once formed, the receptor-ligand bonds are

considered to behave as Hookean springs, with spring constant and rest length denoted by k_{LR} and l_{LR}, respectively.

Due to the densely packed bonds in focal adhesions,[2,3] we postulate that the interface is fully occupied by receptor-ligand pairs, closed bonds or open molecules, with the maximum site density ρ_0 that can be possibly achieved for bond/molecule occupancy. For integrin-based focal adhesions at cell-matrix interface, ρ_0 is usually 10^3-10^4 bonds/molecules per μm^2 that corresponds to 10-30 nm spacing between neighboring ones.[28] The local density of closed receptor-ligand bonds is denoted as ρ_{LR}, which should vary with time due to the aggregation process as well as bond dissociation/association. We proceed by using the normalization scheme: $\rho_{\mathrm{LR}}/\rho_0 = c$, as such c and $(1-c)$ represent the fractions of the closed receptor-ligand bonds and open molecules, respectively.

In the presence of possible bond aggregation facilitated by any non-uniform elastic deformation from the surrounding materials, the interfacial separation h should be modified from a reference value h_0, which corresponds to the uniform interfacial separation when the closed receptor-ligand bonds are evenly distributed at the interface, namely,

$$h(x_1, x_2) = h_0 - u_3(x_1, x_2), \tag{2}$$

where u_3 is the elastic displacement in the direction perpendicular to the interfacial plane, and (x_1, x_2) are Cartesian coordinates attached to the interface.

The total free energy G of the system consists of the terms from both the bulk (denoted as V) and the interface (denoted as A), which can be generally written as

$$G = \int W \, \mathrm{d}V + \int \Gamma \, \mathrm{d}A \,. \tag{3}$$

The first integral extends over the entire volume of the system, W being the elastic energy per unit volume. The second integral extends over the entire interface, Γ being the interfacial energy per unit area. The volumetric term is of the usual form:

$$\int W \, \mathrm{d}V = \frac{1}{2} \int \sigma_{ij} \varepsilon_{ij} \, \mathrm{d}V \,, \tag{4}$$

where σ_{ij} and ε_{ij} are the stress and strain tensors within the bodies of the two opposing materials, both being assumed linearly elastic. Here the repeated indices (i.e., i and j) imply summation over 1 to 3 for all the stress and strain components.

The interfacial term in eqn (3) is contributed by three sources: the elastic energy stored in the stretched or compressed bonds (U_1), the entropic and enthalpic energy of mixing bonds that is commonly represented by a double-well potential (U_2),[29] and the energy associated with the concentration-gradient of distributed bonds (U_3), which is in analogy to that in the Cahn-Hilliard theory of spinodal decomposition of bulk crystals.[30] Therefore,

$$\int \Gamma \, \mathrm{d}A = U_1 + U_2 + U_3 \,, \tag{5}$$

where the elastic, entropic/enthalpic and concentration-gradient terms on the right-hand side can be explicitly expressed as

$$U_1 = \int \frac{1}{2} \rho_0 k_{\mathrm{LR}} c \left(h_0 - u_3 - l_{\mathrm{LR}} \right)^2 \mathrm{d}A \,, \tag{6a}$$

$$U_2 = \int \frac{1}{2}\Omega \rho_0 \beta c^2 (1-c)^2 \, \mathrm{d}A, \tag{6b}$$

$$U_3 = \int \kappa (\nabla c)^2 \, \mathrm{d}A. \tag{6c}$$

Again, all these integrals should be carried out for the entire interface. Ω in eqn (6b) is a numeric parameter measuring the depth of energy well at $c = 0$ or 1,[29] β is a characteristic energy scale associated with any bond redistribution,[31,32] and κ in eqn (6c) describes the magnitude of concentration-gradient effect that has the dimension of energy.[30-32]

The total free energy G can be varied by two concurrent but independent means: the variations in elastic deformation of the two materials and bond redistribution at the interface, denoted as δu_i and δc, respectively. The variation of the total free energy is therefore

$$\begin{aligned} \delta G = & \int \sigma_{ij} \delta u_{i,j} \, \mathrm{d}V - \int \rho_0 k_{\mathrm{LR}} c (h_0 - u_3 - l_{\mathrm{LR}}) \delta u_3 \, \mathrm{d}A \\ & + \int \frac{1}{2} \rho_0 k_{\mathrm{LR}} (h_0 - u_3 - l_{\mathrm{LR}})^2 \, \delta c \, \mathrm{d}A + \int \Omega \rho_0 \beta c (1-c)(1-2c) \delta c \, \mathrm{d}A - \int 2\kappa (\nabla^2 c) \delta c \, \mathrm{d}A \end{aligned}. \tag{7}$$

For bond redistribution itself, the conservation law requires that any variation in local density of closed bonds is owing to the spatial gradient of bond distribution, that is

$$\rho_0 \delta c = -\delta I_{\alpha,\alpha}, \tag{8}$$

where α runs from 1 to 2, representing planar coordinates of the interface, and $\boldsymbol{I}$ is defined as a relocation vector field such that $I_\alpha n_\alpha$ is the number of closed bonds across a unit length of a curve with a unit vector $\boldsymbol{n}$ normal to the curve. Similarly, the rate of change in local density of closed bonds must be equal to the negative of the local flux divergence, namely,

$$\rho_0 \partial c/\partial t = -J_{\alpha,\alpha}, \tag{9}$$

where the flux vector field $\boldsymbol{J}$ is defined in a way that $J_\alpha n_\alpha$ is the closed bond number across a unit length of the curve (unit normal vector: $\boldsymbol{n}$) per unit time. The relation between $\boldsymbol{I}$ and $\boldsymbol{J}$ has been originally described by Suo and Lu[33,34] in modeling stress-driven self-assembly of a binary epilayer. By the virtue of $\boldsymbol{I}$, we can reform the variation in free energy as

$$\begin{aligned}\delta G = &\int \sigma_{ij}\delta u_{i,j}\,\mathrm{d}V - \int \rho_0 k_{\mathrm{LR}} c\left(h_0 - u_3 - l_{\mathrm{LR}}\right)\delta u_3\,\mathrm{d}A \\ &+ \int \frac{\partial}{\rho_0 \partial x_\alpha}\left[\frac{1}{2}\rho_0 k_{\mathrm{LR}}\left(h_0 - u_3 - l_{\mathrm{LR}}\right)^2 + \Omega\rho_0\beta c(1-c)(1-2c) - 2\kappa\nabla^2 c\right]\delta I_\alpha\,\mathrm{d}A\end{aligned}. \tag{10}$$

In general, the mechanical equilibrium can be reached much faster than the chemical equilibrium. Therefore, we can assume the whole system is always in mechanical equilibrium, i.e.,

$$\delta G/\delta u_3 = 0, \tag{11}$$

which recovers the mechanical equilibrium as follows:

$$\sigma_{ij,j} = 0 \text{ (anywhere within } V\text{)}, \tag{12a}$$

$$\sigma_{33} = \rho_0 k_{\mathrm{LR}} c\left(h_0 - u_3 - l_{\mathrm{LR}}\right) \text{ (anywhere at } A\text{)}. \tag{12b}$$

For a reference configuration that the receptor-ligand bonds are uniformly distributed (e.g., $c = c_0$) and therefore the stress is also uniform ($\sigma_{33} = \sigma_0$) at the interface, the combined surface displacement of the opposing materials is simply $u_0 = L\sigma_0/E^*$, where L is a length scale characterizing the thickness of the two materials. It should be noted that L in the preceding formula is assumed to be much larger than any emerging sizes at the interface during bond evolution, as such each of the materials can be accurately

represented as a half-space. The global force balance requires that $\sigma_{33}=\sigma_0$ when $u_3=u_0$, and the boundary condition at the interface (i.e., eqn (12b)) becomes $\sigma_0=\rho_0 k_{\mathrm{LR}} c_0\left(h_0-u_0-l_{\mathrm{LR}}\right)$, by which the uniform surface separation h_0 can be determined as

$$h_0=l_{\mathrm{LR}}+\frac{\sigma_0}{\rho_0 k_{\mathrm{LR}} c_0}+u_0, \tag{13}$$

where the three terms on the right-hand side represent the rest length of bonds, bond deformation and surface displacement of the materials, respectively.

According to the well-known Boussinesq solution,[27] we can relate the surface displacement u_3 to the interfacial traction σ_{33} through

$$u_3\left(x_1,x_2\right)-u_0=\frac{1}{\pi E^*}\iint\frac{\sigma_{33}\left(\xi_1,\xi_2\right)-\sigma_0}{\sqrt{\left(x_1-\xi_1\right)^2+\left(x_2-\xi_2\right)^2}}\mathrm{d}\xi_1\mathrm{d}\xi_2. \tag{14}$$

Substituting the expression of u_3 in terms of σ_{33} (i.e., eqn (12b)) into the integral equation, we obtain

$$\frac{\sigma_0}{\rho_0 k_{\mathrm{LR}} c_0}-\frac{\sigma_{33}}{\rho_0 k_{\mathrm{LR}} c}=\frac{1}{\pi E^*}\iint\frac{\sigma_{33}\left(\xi_1,\xi_2\right)-\sigma_0}{\sqrt{\left(x_1-\xi_1\right)^2+\left(x_2-\xi_2\right)^2}}\mathrm{d}\xi_1\mathrm{d}\xi_2. \tag{15}$$

Together with eqn (15) that governs the mechanical equilibrium, the system is also undergoing dynamic diffusion-type process. We define the driving force F_α for bond relocation process as the free energy reduction associated with one single closed bond moving by a unit distance, namely,

$$\int F_\alpha\,\delta I_\alpha\,\mathrm{d}A=-\delta G, \tag{16}$$

and assume that the local flux is linearly proportional to the driving force by a coefficient M:

$$J_\alpha = M F_\alpha . \tag{17}$$

In addition to the diffusion term described by the flux of the closed receptor-ligand bonds J_α, the local binding and unbinding events of receptor-ligand bonds also contribute to the local change of closed bond density. We end up with a separate governing equation, which is time-varying, as

$$\frac{\partial c}{\partial t} = \frac{M}{\rho_0^2}\nabla^2\left[\frac{1}{2}\rho_0 k_{\mathrm{LR}}\left(h_0 - u_3 - l_{\mathrm{LR}}\right)^2 + \Omega\rho_0\beta c(1-c)(1-2c) - 2\kappa\nabla^2 c\right] + k_{\mathrm{on}}(1-c) - k_{\mathrm{off}}\, c\,, \tag{18}$$

where the last two terms represent kinetic reaction due to bond association and dissociation, with k_{on} and k_{off} being the association rate of open bonds and dissociation rate of closed bonds, respectively. We further assume that the dissociation rate depends on bond traction σ_{33} and behaves like catch-slip bonds, as described by the classical two-pathway model:[35-37]

$$k_{\mathrm{off}} = k_{\mathrm{c}}^0 \exp\left(-\sigma_{33}/\sigma_{\mathrm{c}}\right) + k_{\mathrm{s}}^0 \exp\left(\sigma_{33}/\sigma_{\mathrm{s}}\right), \tag{19}$$

where k_{c}^0 and k_{s}^0 are the rate coefficients for the 'catch' and 'slip' pathways at zero force, respectively; σ_{c} and σ_{s} are the stress constants that measure the sensitivity of bond dissociation rate on traction level for the two pathways. If $k_{\mathrm{c}}^0 = 0$, the force dependence of dissociation kinetics in eqn (19) immediately reduces to the slip bond model, as first proposed by Bell.[38] The association rate is assumed to depend on the separation distance between the molecular-bearing surfaces as[39,40]

$$k_{\mathrm{on}} = k_{\mathrm{on}}^0 \exp\left(-\left(h_0 - u_3\right)^2 / x_0^2\right), \tag{20}$$

where k_{on}^{0} is the rate constant and x_0 is the characteristic length scale measuring how fast bond association decays with increasing surface separation.

3 Results and Discussion

In simulating the dynamics of bond aggregation, a sufficiently large region of the interface is initially joined via randomly dispersed receptor-ligand bonds ($c = c_0$). We proceed by choosing two dimensionless quantities

$$a = \sqrt{\frac{\kappa}{\rho_0 \beta}}, \ \tau = \frac{\kappa}{M\beta^2} \tag{21}$$

as the basic length and time scales in the analysis. Taking $\kappa = 10^{-17}$ J , $\beta = 1000\, k_{\text{B}}T$ ($k_{\text{B}}T$: Boltzmann's constant multiplied by the absolute temperature), $\rho_0 = 1000/\mu\text{m}^2$ and $M = 10^{18}$ $\text{J}^{-1}\text{s}^{-1}$, a and τ are estimated to be 50 nm and 0.625 s, respectively. Normalizing all the lengths in the governing equations (eqn (15) and (18)) by a, times by τ, rates by τ^{-1} and stresses by $\rho_0\beta/a$ leads to

$$\frac{\hat{\sigma}_0}{c_0} - \frac{\hat{\sigma}_{33}}{c} = \frac{q_1 q_2}{\pi} \iint \frac{\hat{\sigma}_{33}\left(\hat{\xi}_1, \hat{\xi}_2\right) - \hat{\sigma}_0}{\sqrt{\left(\hat{x}_1 - \hat{\xi}_1\right)^2 + \left(\hat{x}_2 - \hat{\xi}_2\right)^2}} \mathrm{d}\hat{\xi}_1 \mathrm{d}\hat{\xi}_2, \tag{22a}$$

$$\frac{\partial c}{\partial \hat{t}} = \nabla^2 \left(\frac{q_1}{2} \left(\hat{h}_0 - \hat{u}_3 - \hat{l}_{\text{LR}} \right)^2 + \Omega c(1-c)(1-2c) - 2\nabla^2 c \right) + \hat{k}_{\text{on}}(1-c) - \hat{k}_{\text{off}}\, c, \tag{22b}$$

where the hats indicate dimensionless quantities, $\hat{h}_0 = \hat{l}_{\text{LR}} + q_2 q_3 \sigma_0 + \hat{\sigma}_0/(q_1 c_0)$, and

$$q_1 = \frac{k_{\mathrm{LR}} a^2}{\beta},\ q_2 = \frac{\rho_0 \beta}{E^* a},\ q_3 = \frac{L}{a} \tag{23}$$

are three dimensionless parameters in the problem. q_1 combines factors such as the bond stiffness (k_{LR}), the concentration-gradient effect (κ), the site density (ρ_0) and q_2 represents the effects from material compliance through E^*.

The intention here is to illustrate the model predictions and implications for cellular focal adhesion using representative parameters, and a complete survey of the full parameter space is unattractive. From $a = 50\,\mathrm{nm}$, $\beta = 1000\,k_{\mathrm{B}}T$ and $k_{\mathrm{LR}} = 0.32\,\mathrm{pN/nm}$,[41] we take q_1 to be 0.2; $\rho_0 = 1000/\mu\mathrm{m}^2$ and $E^* = 0.8\,\mathrm{MPa}$ lead to $q_2 = 0.1$;[28,42] q_3 is set to be 100 to represent a much thicker bi-material than the feature size at the interface (for validity of the half-space assumption). Ω is set to be 2.2. Other representative values for bond kinetics are chosen as: $\hat{\sigma}_0 = 0.005$, $\hat{k}_{\mathrm{on}}^0 = 0.005$, $\hat{k}_{\mathrm{s}}^0 = 0.001$, $\hat{k}_{\mathrm{c}}^0 = 0.003$, $\hat{\sigma}_{\mathrm{s}} = 0.01$ and $\hat{\sigma}_{\mathrm{c}} = 0.0025$.[35-40] The same set of parameters is used for all the simulation cases unless specified otherwise.

Eqn (22a) is an integral equation which cannot be solved directly. To avoid the difficulty, we follow the gradient flow method[43] so that the equation can be rewritten as

$$\frac{\partial \hat{\sigma}_{33}}{\partial \hat{t}} = -\Pi \left[\frac{q_1 q_2}{\pi} \iint \frac{\hat{\sigma}_{33}\left(\hat{\xi}_1, \hat{\xi}_2\right) - \hat{\sigma}_0}{\sqrt{\left(\hat{x}_1 - \hat{\xi}_1\right)^2 + \left(\hat{x}_2 - \hat{\xi}_2\right)^2}} \mathrm{d}\hat{\xi}_1 \mathrm{d}\hat{\xi}_2 - \left(\frac{\hat{\sigma}_0}{c_0} - \frac{\hat{\sigma}_{33}}{c} \right) \right], \tag{24}$$

where Π is a kinetic coefficient characterizing the relaxation rate of the stress field. Once $\partial \hat{\sigma}_{33}/\partial \hat{t}$ decreases to zero, eqn (22a) will be automatically satisfied. We apply Fourier transform to eqn (22a) and (22b) and solve them in the Fourier space, as performed in previous studies.[33,34] In each time step, we

first evolve eqn (24) for given bond density c until the mechanical equilibrium is reached (i.e., $\partial\hat{\sigma}_{33}/\partial\hat{t}=0$). Eqn (22b) is then solved to obtain the time evolution of bond density distribution. In all of our simulations, the coupled equations are solved in a square domain of size 256×256, a range found to be adequate for numerical purpose, and periodical boundary conditions are maintained.

Five simulation snapshots are shown in Fig. 2a to 2e, where the extent of bond clustering is examined by its deviation up to $t=10{,}000\,\tau$ from a random distribution around $c=0.4$ at $t=0$. Fig. 2f plots the change of average cluster size over the simulation time. As the system evolves, the interfacial bonds that are initially random aggregate into clustered domains, which finally settle at a feature size in a triangular lattice. The clustering process reaches a steady-state by $t=5{,}000\,\tau$ that corresponds to ~1 hour in real dimension, beyond which the spatial bond distribution becomes almost invariant. Domains with similar ordered pattern have been observed in other self-assembled systems on two dimensional surfaces, such as molecules on dielectric substrates,[44] Langmuir monolayers,[45] and block coploymers.[46]

The displacement profile $\hat{u}_3$ and the stress field $\hat{\sigma}_{33}$ at the steady-state of the spatial-temporal evolution are shown in Fig. 3a and 3b, respectively, both exhibiting dotted pattern identical to the spatial distribution of bonds in Fig. 2. The size of the bond clusters is found to be ~20 (Fig. 3b), corresponding to ~1 μm in real space by recalling the length scale $a=50\,\text{nm}$. In addition, the stress level within individual adhesion spots is about 0.012, which can be converted to ~1 kPa via the stress scale $\rho_0\beta/a=80\,\text{kPa}$. All these predicted values are essentially consistent with those measured in focal adhesions.[2,3,19,20] The closed bond density and bond stress are monitored in the time sequence of the simulation for three representative points, A, B and C as marked in Fig. 3b, which evolve into cluster center, cluster rim and valley between clusters, respectively, in comparison with the corresponding average over the entire interface (Fig. 3c and 3d). Averaging over the entire interface, both closed bond

density and bond stress decrease when the system reaches its steady state from the initial condition, which reflects the competition between bond dissociation and association in the aggregation process for the selected parameters.

Recently, catch-slip bond behavior has been demonstrated for integrin-ligand bonds that are responsible for cell-matrix adhesion,[37] in contrast to Bell's slip bond description.[38] It is therefore interesting to examine the chemo-mechanical process of bond aggregation in terms of these two different bond types. Strikingly, for catch-slip molecular bonds, the applied stress tends to coarsen the clusters until an optimal load level that leads to maximized bond clusters (Fig. 4a); while for slip bonds, the increasing applied stress monotonically refines the pattern into smaller clusters (Fig. 4b). Experiments have found that the size of mature FAs reversibly changes in proportion to the magnitude of applied stress below a threshold value,[19,20] and our results predict that integrin's catch-slip behavior is the key accounting for such phenomenon. To further investigate the completion between different time scales, we keep the diffusion term constant and vary the bond reaction term by changing $\hat{k}_{\mathrm{on}}^{0}$, $\hat{k}_{\mathrm{s}}^{0}$ and $\hat{k}_{\mathrm{c}}^{0}$ proportionally to achieve nominally identical competition between bond dissociation and association. The relation between cluster size and applied stress is found to be biphasic for catch-slip bond but monotonic for slip bond for all the cases studied, and faster reaction kinetics (compared to diffusion) generally results in smaller bond clusters (Fig. 4).

In Fig. 5, the average size of bond cluster is plotted as a function of q_1 and q_2 for different values of $\hat{\sigma}_0$, where the average cluster size is measured from individual clusters when the catch-slip bond system evolves to its steady-state. The feature size of bond clusters is predicted to be enlarged for increasing q_1 contributed by factors such as stronger concentration-gradient effect (κ), stiffer bonds (k_{LR}) and lower site density (ρ_0), as indicated in Fig. 5a. The cluster size also decreases as the

neighboring materials become more compliant in Fig. 5b (E^* is changed from 800 to 67 kPa as q_2 increases from 0.1 to 1.2), consistent with the experimental trend that focal adhesions are impaired on substrates that are highly compliant.[13,14]

Interestingly, it may be recognized that

$$q_1 q_2 = \frac{\rho_0 k_{\mathrm{LR}} a}{E^*}, \tag{25}$$

which bears the similar form of so-called stress concentration index that has been proposed to govern the stress distribution within molecular bond clusters.[47] Roughly speaking, the index $q_1 q_2$ represents the stiffness of the layer of interfacial bonds relative to the modulus of surrounding bulk materials. According to the previous analysis,[47] the stress distribution should be nearly uniform within individual bond clusters when the index is much smaller than unity, and become highly concentrated at the cluster edges otherwise. This is indeed observed in Fig. 6.

4 Conclusions

In summary, we have theoretically developed a mechanochemical framework that governs the spatial-temporal evolution of interfacial receptor-ligand bonds in the coupled elastic field and chemical potential. The governing partial differential equations are solved numerically and the time-varying behaviors of bond aggregation are obtained, with emerging cluster size regulated by material compliance and applied load. With specified diffusion and reaction kinetics of interfacial bonds, the model should be applicable to integrin-based cell-matrix adhesions as well as cadherin-based cell-cell junctions. Upon the previous modeling work by Wang and Gao,[24] the major progress this study made lies in the following

aspects: i) it extends the mechanochemical process of bond patterning from one-dimensional along a line to two-dimensional across an interface; ii) the present model presents the real-time evolution of the bond aggregation process rather than a perturbation analysis on system energy; iii) the kinetic processes of de-bonding and re-bonding, which are strongly coupled to the elastic field through traction and displacement, are incorporated into the analysis.

Several important aspects of the problem have been neglected in the present study, which certainly warrant future investigation. For one thing, closed bonds are allowed to diffuse in order to capture the bond translocation at the interface between cell and natural ECM, or between cell and cell, where the ligands can be considered mobile. For the case that ligand molecules are less mobile on the surfaces of artificial ECM, we assume in the model that closed receptor-ligand bonds can still switch positions with their neighbors because of lateral extensibility of ligand molecules, and there is no extra energy associated with this lateral extensibility. Notice that no length scale is required for position switching in our continuum description, so there is no problem for bond translocation to occur even the lateral extensibility of ligand is very limited. Of course, one can achieve easy or difficult bond translocation by choosing the value of M in eqn (17). More studies can be performed to account for the role of immobilized and patterned ligands in cell-ECM interaction. The present model is idealized that the interface of molecule bonds between two semi-infinite homogeneous materials is subjected to uniform traction, resulting in rather regular lattice of bond clusters (Fig. 2 and 3). In reality, focal adhesions between cell and matrix can be influenced by many factors that lead to non-uniformly distributed cluster patterns. For example, cellular traction can be non-uniform at cell-matrix interface, materials can bear some inhomogeneity, geometric features may exist at the interface and/or within the materials, etc.

The modeling framework developed here has captured the combined behavior of size emergence, stiffness dependence and loading effects in the dynamic formation of adhesion domain, which may help to understand cell-matrix adhesion that contains convoluted time scales from bond transport and reaction, both regulated by the mechanical field. The stiffness of surrounding materials is predicted to benefit the growth of focal adhesions, and the clusters of integrin bonds enlarge with increasing magnitude of applied stress, up to a threshold value. In spite of the simplification in certain aspects, it is encouraging that the key predictions of such an idealized model are quantitatively consistent with relevant experiments. We anticipate that the general framework here will initiate modeling and experiments to investigate more sophisticated mechanical and geometrical properties of cell-matrix system, such as material anisotropy,[48] heterogeneity,[49] pretension[50] and finite dimension of cell-matrix that give rise to inherent non-uniformity, which exert influence on molecular adhesion at the interfaces and may guide the design of artificial materials to control adhesion-mediated cellular behaviors.

Acknowledgements

This work was supported by the "Thousand Young Talents Program" of China (to H.J. and J.Q.), the National Natural Science Foundation of China (11342010 and 11472271 to H.J., 11202184 and 11321202 to J.Q.), and the Fundamental Research Funds for Central Universities of China (2014FZA4027).

References

1 B. Geiger and A. Bershadsky, *Curr. Opin. Cell Biol.*, 2001, **13**, 584.

2 E. Zamir, M. Katz, Y. Posen, N. Erez, K. M. Yamada, B. Z. Katz, S. Lin, D. C. Lin, A. Bershadsky, Z. Kam and B. Geiger, *Nat. Cell Biol.*, 2000, **2**, 191.

3 R. Zaidel-Bar, C. Ballestrem, Z. Kam and B. Geiger, *J. Cell Sci.*, 2003, **116**, 4605.

4 B. Alberts, A. Johnson, J. Lewis, M. Raff, K. Roberts and P. Walter, *Molecular Biology of the Cell*, Garland Science, New York, 2002.

5 T. Erdmann and U. S. Schwarz, *Phys. Rev. Lett.*, 2004, **92**, 108102.

6 T. Erdmann and U. S. Schwarz, *J. Chem. Phys.*, 2004, **121**, 8997.

7 J. Qian, J. Wang and H. Gao, *Langmuir*, 2008, **24**, 1262.

8 J. Qian, J. Z. Wang, Y. Lin and H. J. Gao, *Biophys. J.*, 2009, **97**, 2438.

9 Y. Lin and L. B. Freund, *Phys. Rev. E*, 2008, **78**, 021909.

10 N. Nisenholz, K. Rajendran, Q. Dang, H. Chen, R. Kemkemer, R. Krishnan and A. Zemel, *Soft Matter*, 2014, **10**, 7234.

11 N. G. Genes, J. A. Rowley, D. J. Mooney and L. J. Bonassar, *Arch. Biochem. Biophys.*, 2004, **422**, 161.

12 A. J. Engler, M. A. Griffin, S. Sen, C. G. Bonnetnann, H. L. Sweeney and D. E. Discher, *J. Cell Biol.*, 2004, **166**, 877.

13 R. J. Pelham and Y. L. Wang, *Proc. Natl. Acad. Sci. U.S.A.*, 1997, **94**, 13661.

14 G. K. Xu, C. Yang, J. Du and X. Q. Feng, *J. Biomech.*, 2014, **47**, 1479.

15 J. Lober, F. Ziebert and I. S. Aranson, *Soft Matter*, 2014, **10**, 1365.

16 C. M. Lo, H. B. Wang, M. Dembo and Y. L. Wang, *Biophys. J.*, 2000, **79**, 144.

17 M. L. Gardel, J. H. Shin, F. C. MacKintosh, L. Mahadevan, P. Matsudaira and D. A. Weitz, *Science*, 2004, **304**, 1301.

18 C. Storm, J. J. Pastore, F. C. MacKintosh, T. C. Lubensky and P. A. Janmey, *Nature*, 2005, **435**, 191.

19 D. Riveline, E. Zamir, N. Q. Balaban, U. S. Schwarz, T. Ishizaki, S. Narumiya, Z. Kam, B. Geiger and A. D. Bershadsky, *J. Cell Biol.*, 2001, **153**, 1175.

20 N. Q. Balaban, U. S. Schwarz, D. Riveline, P. Goichberg, G. Tzur, I. Sabanay, D. Mahalu, S. Safran, A. Bershadsky, L. Addadi and B. Geiger, *Nat. Cell Biol.*, 2001, **3**, 466.

21 A. S. Sarvestani, *Soft Matter*, 2013, **9**, 5927.

22 T. R. Weikl and R. Lipowsky, *Biophys. J.*, 2004, **87**, 3665.

23 M. J. Paszek, D. Boettiger, V. M. Weaver and D. A. Hammer, *PLoS Comput. Biol.*, 2009, **5**, e1000604.

24 J. Z. Wang and H. J. Gao, *J. Mech. Phys. Solids*, 2008, **56**, 251.

25 P. Kanchanawong, G. Shtengel, A. M. Pasapera, E. B. Ramko, M. W. Davidson, H. F. Hess and C. M. Waterman, *Nature*, 2010, **468**, 580.

26 J. Du, X. F. Chen, X. D. Liang, G. Y. Zhang, J. Xu, L. R. He, Q. Y. Zhan, X. Q. Feng, S. Chien and C. Yang, *Proc. Natl. Acad. Sci. U.S.A.*, 2011, **108**, 9466.

27 K. L. Johnson, *Contact Mechanics*, Cambridge University Press, Cambridge, 1985.

28 M. Arnold, E. A. Cavalcanti-Adam, R. Glass, J. Blummel, W. Eck, M. Kantlehner, H. Kessler and J. P. Spatz, *ChemPhysChem*, 2004, **5**, 383.

29 K. A. Dill and S. Bromberg, *Molecular Driving Forces: Statistical Thermodynamics in Chemistry and Biology*, Garland Science, New York, 2002.

30 J. W. Cahn and J. E. Hilliard, *J. Chem. Phys.*, 1958, **28**, 258.

31 H. Y. Jiang and T. R. Powers, *Phys. Rev. Lett.*, 2008, **101**, 018103.

32 H. Y. Jiang, *Phys. Rev. Lett.*, 2012, **109**, 198101.

33 Z. Suo and W. Lu, *J. Mech. Phys. Solids*, 2000, **48**, 211.

34 W. Lu and Z. Suo, *J. Mech. Phys. Solids*, 2001, **49**, 1937.

35 Y. V. Pereverzev, O. V. Prezhdo, M. Forero, E. V. Sokurenko and W. E. Thomas, *Biophys. J.*, 2005, **89**, 1446.

36 K. K. Sarangapani, J. Qian, W. Chen, V. I. Zarnitsyna, P. Mehta, T. Yago, R. P. McEver and C. Zhu, *J. Biol. Chem.*, 2011, **286**, 32749.

37 F. Kong, A. J. Garcia, A. P. Mould, M. J. Humphries and C. Zhu, *J. Cell Biol.*, 2009, **185**, 1275.

38 G. I. Bell, *Science*, 1978, **200**, 618.

39 L. Sun, Q. H. Cheng, H. J. Gao and Y. W. Zhang, *Phys. Rev. E*, 2009, **79**, 061907.

40 L. Sun, Q. H. Cheng, H. J. Gao and Y. W. Zhang, *J. R. Soc. Interfac*e, 2012, **9**, 928.

41 W. Chen, J. Z. Lou, E. A. Evans and C. Zhu, *J. Cell Biol.*, 2012, **199**, 497.

42 D. E. Discher, P. Janmey and Y. L. Wang, *Science*, 2005, **310**, 1139.

43 Y. Ni and A. K. Soh, *Acta Mater.*, 2014, **69**, 37.

44 Z. Suo and W. Hong, *Proc. Natl. Acad. Sci. U.S.A.*, 2004, **101**, 7874.

45 M. Seul and D. Andelman, *Science*, 1995, **267**, 476.

46 T. M. Parker, L. K. Wilson, N. G. Condon and F. M. Leibsle, *Phys. Rev. B*, 1997, **56**, 6458.

47 H. J. Gao, J. Qian and B. Chen, *J. R. Soc. Interfac*e, 2011, **8**, 1217.

48 W. L. Zhang, Y. Lin, J. Qian, W. Q. Chen and H. J. Gao, *Adv. Funct. Mater.*, 2013, **23**, 4729.

49 W. L. Zhang, J. Qian, H. M. Yao, W. Q. Chen and H. J. Gao, *Sci. China Phys. Mech.*, 2012, **55**, 980.

50 S. J. He, Y. W. Su, B. H. Ji and H. J. Gao, *J. Mech. Phys. Solids*, 2014, **70**, 116.

Figure Captions

Fig. 1 Schematic of the bond aggregation model under investigation. (*a*) Two semi-infinite elastic materials joined via receptor-ligand bonding at the interface against an externally applied tensile stress. (*b*) Bond transition between closed and open states with traction-dependent dissociation and separation-dependent association rates. (*c*) Diffusion of receptor-ligand bonds across the interface.

Fig. 2 (*a-e*) Temporal snapshots of the closed bond density distribution (i.e., c) starting with a random pattern at the interface. The initial distribution is around an average value of $c = 0.4$ with random fluctuations within 0.1. A square domain of size 256×256 and periodical boundary conditions are adopted in the simulation. (*f*) The time-varying behavior of average cluster size in the simulation. The involved parameters are chosen as: $q_1 = 0.2$, $q_2 = 0.1$, $q_3 = 100$, $\hat{\sigma}_0 = 0.005$, $\hat{k}_{\text{on}}^0 = 0.005$, $\hat{k}_{\text{s}}^0 = 0.001$, $\hat{k}_{\text{c}}^0 = 0.003$, $\hat{\sigma}_{\text{s}} = 0.01$ and $\hat{\sigma}_{\text{c}} = 0.0025$.

Fig. 3 The spatial-temporal evolution of the mechanical and biochemical processes in bond aggregation. (*a*) The displacement profile $\hat{u}_3$ and (*b*) the interfacial stress $\hat{\sigma}_{33}$ of the steady-state at $t = 10{,}000\,\tau$. The time-varying behavior of (*c*) the close bond density and (*d*) the bond stress for three representative points (A, B and C marked in (*b*)) that evolve into cluster center, cluster rim and valley between clusters, respectively, in comparison with the corresponding average over the entire interface. The parameters used in this simulation are the same as those in Fig. 2.

Fig. 4 The average size of bond clusters as a function of $\hat{\sigma}_0$ for different $\hat{k}_{\text{on}}^0$ when individual molecular bonds exhibit (*a*) the catch-slip behavior and (*b*) slip behavior, respectively. The cluster sizes are measured by averaging the areas of individual clusters when the system evolves to its steady-state after

the period of $50{,}000\,\tau$. $\hat{k}_{\mathrm{s}}^{0}$ and $\hat{k}_{\mathrm{c}}^{0}$ are varying in proportion to $\hat{k}_{\mathrm{on}}^{0}$ without altering the nominal ratio of bond dissociation to association for all the cases studied. The error bars represent standard deviation.

Fig. 5 The average size of bond clusters, measured by averaging the areas of individual clusters at steady-state ($t = 50{,}000\,\tau$), as a function of (*a*) q_1 and (*b*) q_2 for different values of $\hat{\sigma}_0$ for catch-slip bond system. The error bars represent standard deviation.

Fig. 6 The steady-state distributions of the normalized bond stress ($\hat{\sigma}_{33}$) within individual bond clusters, governed by the stress concentration index, i.e., $q_1 q_2$. (*a*) $q_1 = 0.2$, $q_2 = 0.1$, $\hat{\sigma}_0 = 0.003$ and (*b*) $q_1 = 2$, $q_2 = 1$, $\hat{\sigma}_0 = 0.003$. (*c*) and (*d*) show the traction distribution along a straight line at the interface, marked in (*a*) and (*b*), respectively. This result indicates a transition between uniform and crack-like singular distributions of the interfacial bond traction.

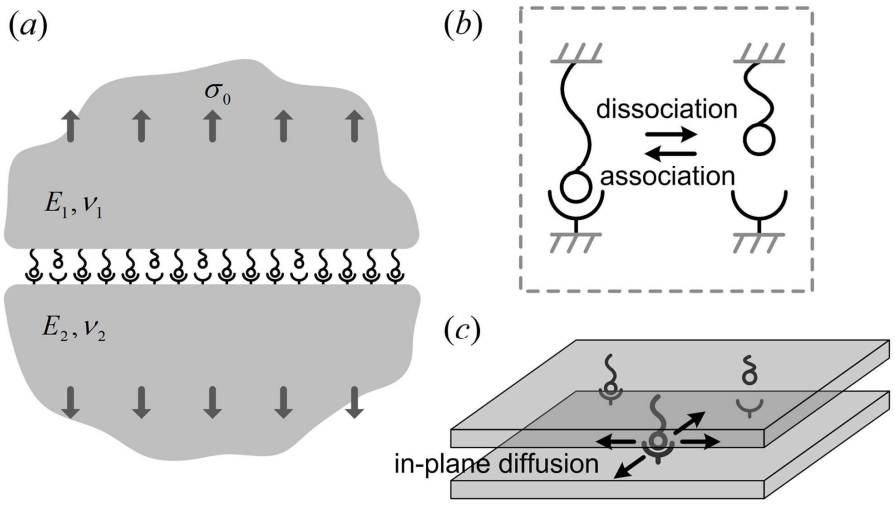

Fig. 1

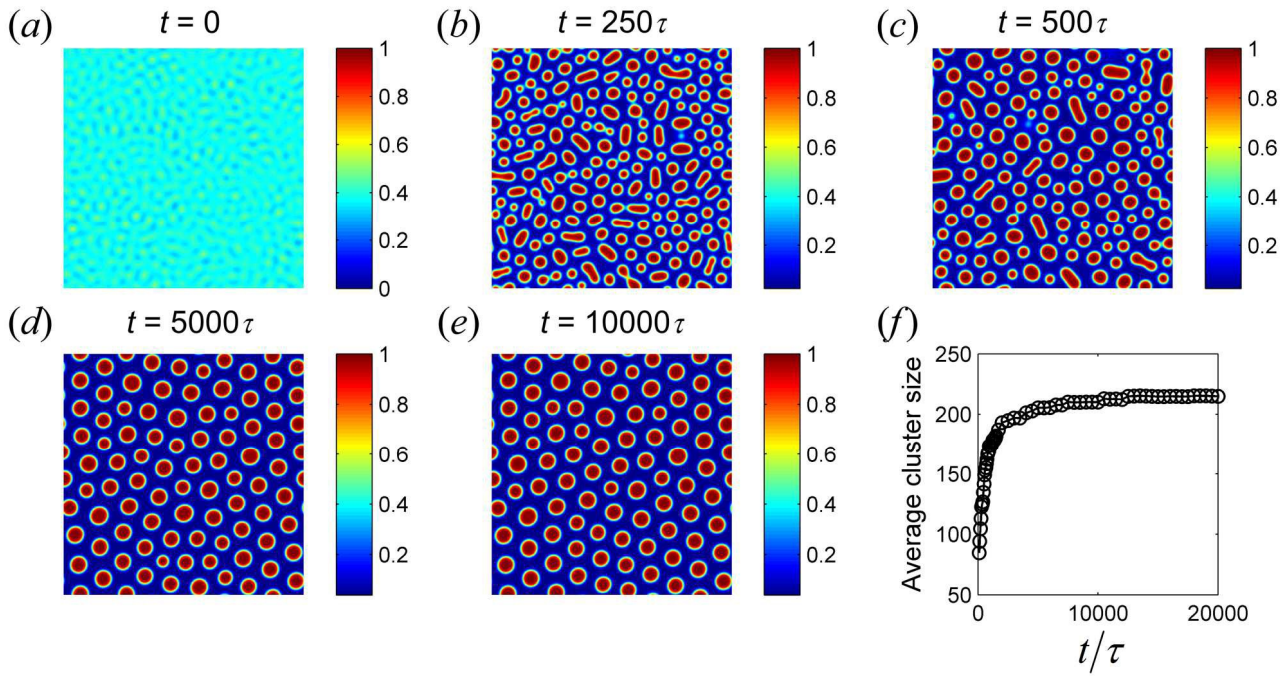

Fig. 2

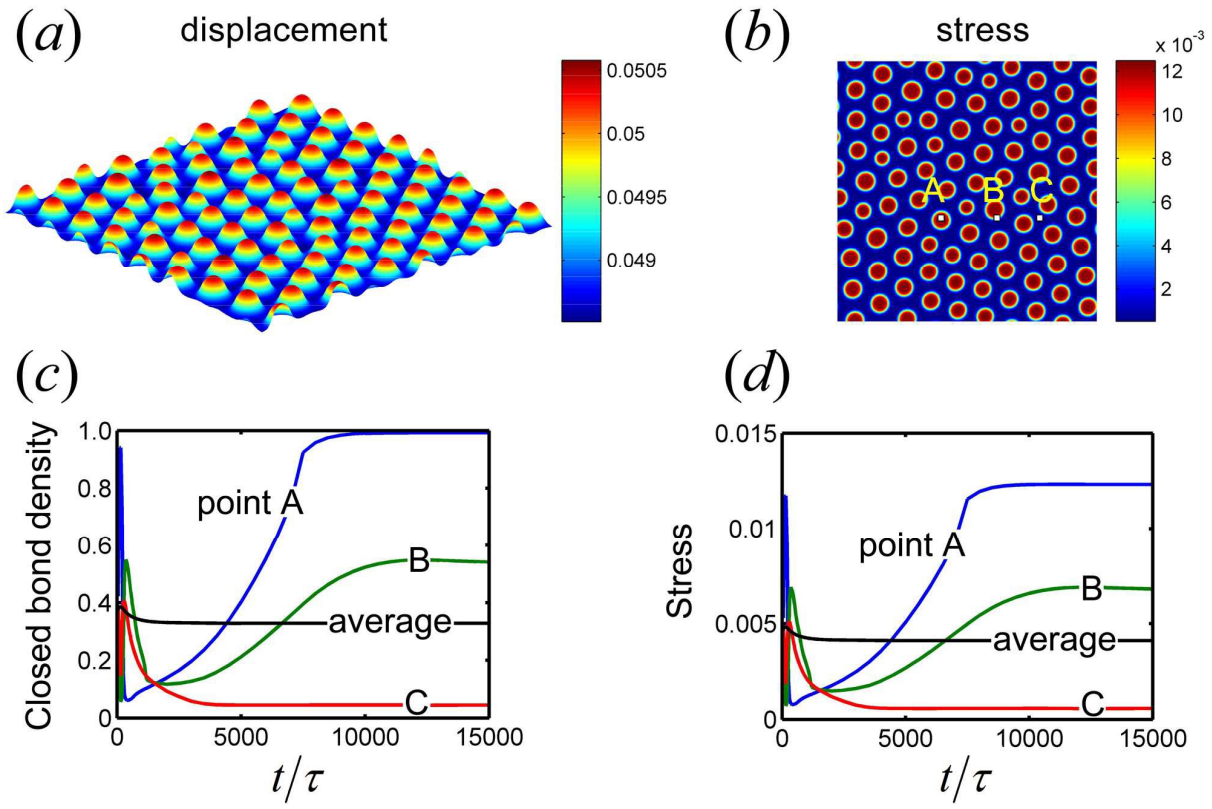

Fig. 3

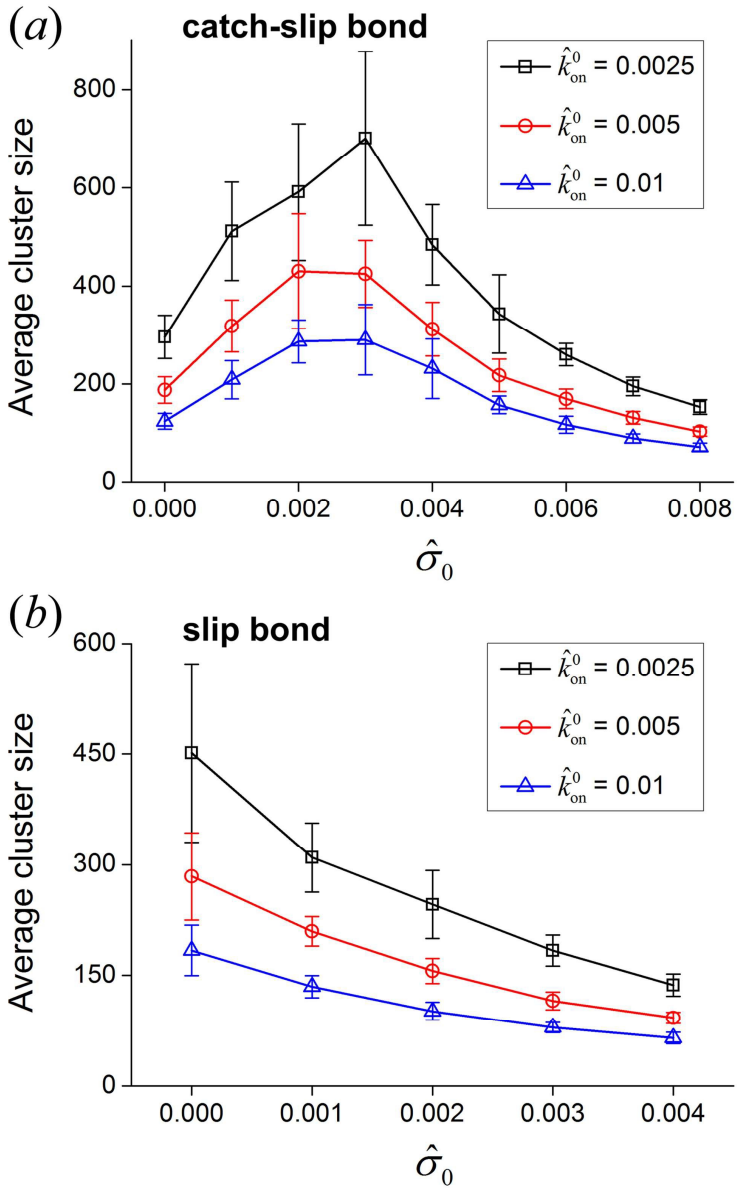

Fig. 4

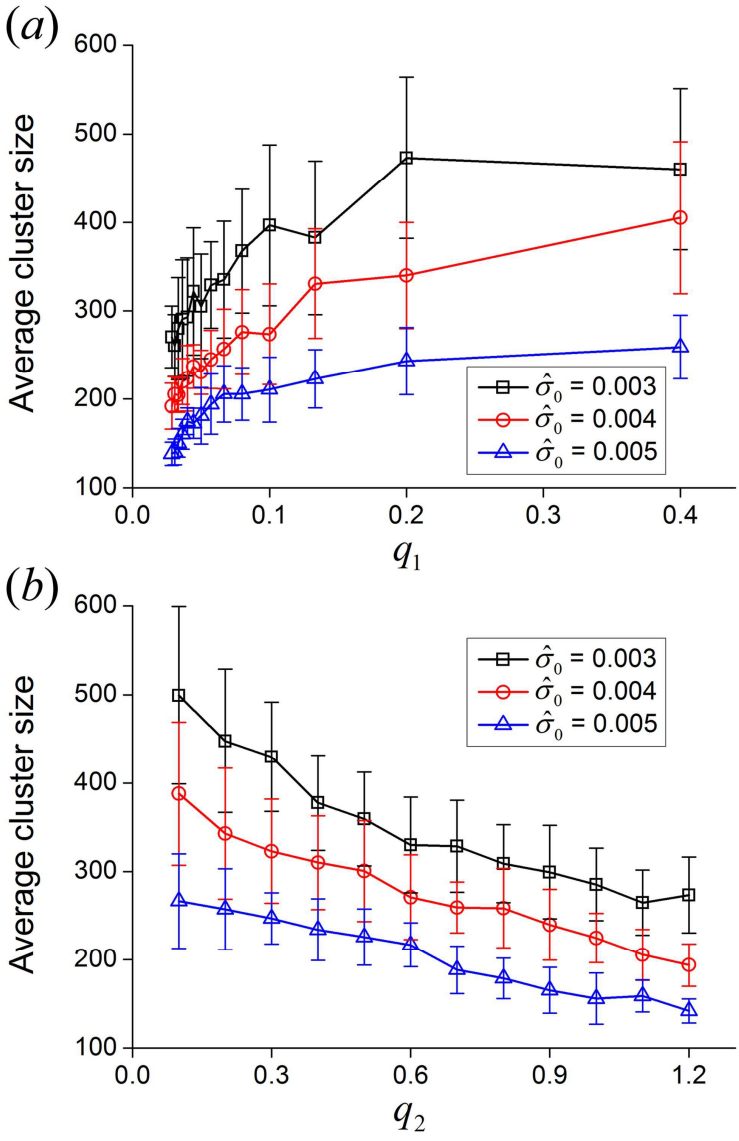

Fig. 5

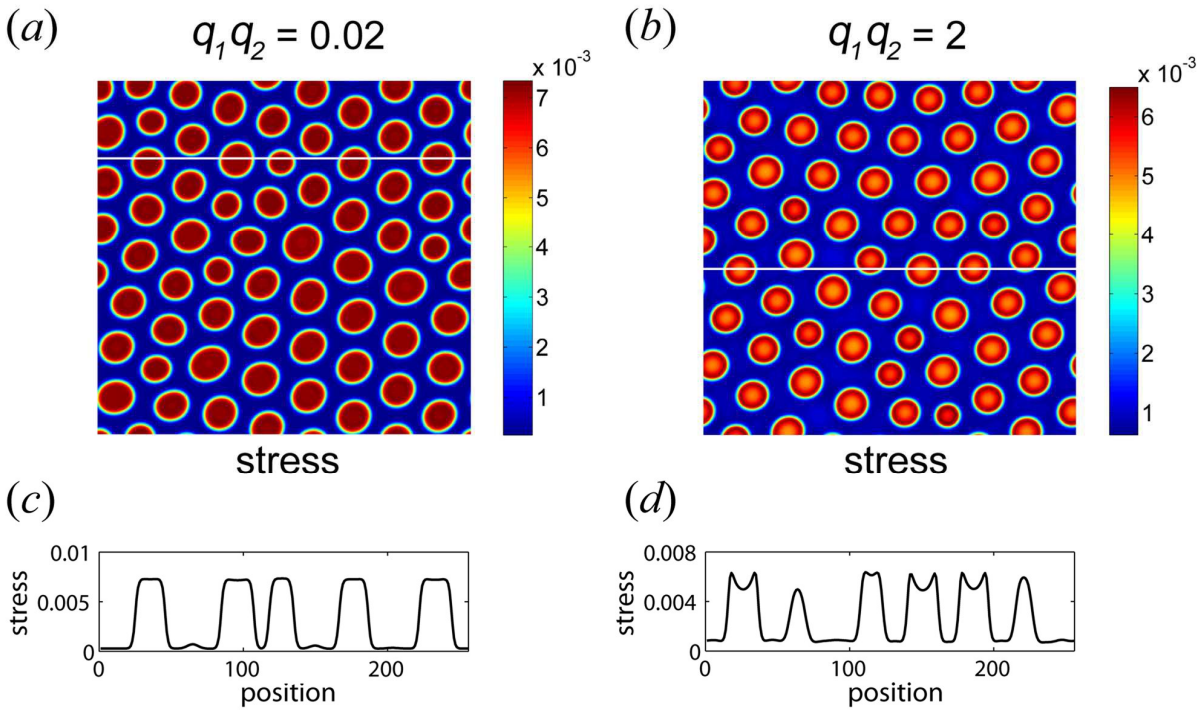

Fig. 6